

# Reduction of the electrocaloric entropy change of ferroelectric $\text{PbZr}_{1-x}\text{Ti}_x\text{O}_3$ epitaxial layers due to an elastocaloric effect

Trong Tong,\* J. Karthik, R. V. K. Mangalam, Lane W. Martin, and David G. Cahill

*Department of Materials Science and Engineering and Materials Research Laboratory, University of Illinois, Urbana, Illinois 61801 USA*

(Received 27 January 2014; revised manuscript received 24 August 2014; published 26 September 2014)

We report laser-based direct measurements of the pyroelectric and electrocaloric effects of  $\text{PbZr}_{1-x}\text{Ti}_x\text{O}_3$  epitaxial layers as a function of temperature and electric field. By evaluating the differences between the total pyroelectric and electrocaloric coefficients, we determine the secondary contribution to the electrocaloric effect that is created by a combination of piezoelectric and elastocaloric effects. The secondary contribution to the electrocaloric coefficient has the opposite sign as the primary effect and therefore reduces the overall entropy change of  $\text{PbZr}_{1-x}\text{Ti}_x\text{O}_3$  in an electric field. The absolute magnitude of the secondary effect is comparable to the primary effect at elevated temperatures of  $\approx 200^\circ\text{C}$ .

DOI: [10.1103/PhysRevB.90.094116](https://doi.org/10.1103/PhysRevB.90.094116)

PACS number(s): 77.55.Kt, 77.55.hj, 77.55.Px, 77.70.+a

## I. INTRODUCTION

Heat engines convert thermal energy to work and pump heat against a temperature gradient. While most practical heat engines are based on the large entropy difference between the vapor and condensed phases of a working fluid, there is increasing interest in using the physics of materials to build efficient solid-state heat engines. For example, thermoelectric generators use the entropy of charge carriers in semiconductors to convert a steady flow of heat to electrical power. Caloric effects in which the entropy of a material changes in response to an external field have potential application in energy scavenging and solid-state refrigeration [1,2].

Our work is focused on the electrocaloric effect where the entropy of a material is modulated by an electric field. While the inverse of the electrocaloric effect, the pyroelectric effect, has been widely studied, the electrocaloric effect is less studied, due in part to the significant experimental challenge of direct measurements of the temperature change.

The total pyroelectric coefficient can be described as the sum of primary and secondary contributions [3]:

$$\Pi = \frac{dP}{dT} = \Pi' + \Pi'', \quad (1)$$

where  $P$  is the electrical polarization and  $T$  is temperature. The primary pyroelectric coefficient  $\Pi' = (\frac{dP}{dT})_{E,\varepsilon}$  describes the change of polarization with respect to temperature at constant strain ( $\varepsilon$ ) and electric field ( $E$ ). The secondary pyroelectric coefficient,  $\Pi'' = \sum_i d_{ijk}^* c_{jklm} \alpha_{lm}$ , is the contribution to the change in polarization from thermal expansion combined with the piezoelectric effect [3]. Here,  $d_{ijk}^*$  is the direct piezoelectric coefficient; the notation of the superscript asterisk is typically used to differentiate the direct piezoelectric coefficient from the converse piezoelectric coefficient  $d_{ijk}$ .  $c_{jklm}$  is the fourth-rank elastic constant tensor, and  $\alpha_{lm}$  is the second-rank thermal expansion coefficient tensor. For materials with tetragonal symmetry and replacing the fourth-rank tensor notation with conventional two-index notation,  $\Pi''$  is [3]

$$\Pi'' = 2\alpha_1(d_{31}^*c_{11} + d_{31}^*c_{12} + d_{33}^*c_{13}) + \alpha_3(2d_{31}^*c_{13} + d_{33}^*c_{33}). \quad (2)$$

As discussed below, in our experiment, the lateral expansion of the lead zirconate titanate (PZT) layers is zero because the films are confined by the substrate. Hence, the secondary coefficient reduces to  $\Pi'' = d_{33}^*c_{33}\alpha_3$ . Generally,  $d_{33}^*$  is positive for PZT films [4], hence  $\Delta E = E_2 - E_1$  while  $\Pi' < 0$ .

Similarly, we separate the total electrocaloric coefficient into the primary and secondary contributions:

$$\Sigma = \frac{dS}{dE} = \Sigma' + \Sigma'', \quad (3)$$

where  $S$  is entropy and  $E$  is the electric field. The primary electrocaloric coefficient  $\Sigma' = (\frac{dS}{dE})_{T,\varepsilon}$  describes the change of entropy in response to an applied field at constant strain and temperature. The secondary coefficient,  $\Sigma'' = \sum_i C d_{ijk} \gamma_{jk}$ , results from changes in the vibrational entropy created by the elastic strain due to the piezoelectric effect [5]. Here,  $\gamma_{jk}$  is the generalized Grüneisen parameter tensor that relates changes in stress to changes in internal energy at constant strain for an anisotropic material [6],  $d_{ijk}$  is the converse piezoelectric coefficient, and  $C$  is the volumetric heat capacity at constant volume. For tetragonal symmetry

$$\Sigma'' = C(2d_{31}\gamma_1 + d_{33}\gamma_3). \quad (4)$$

Here  $\gamma_1 = \frac{1}{C}(c_{11}\alpha_1 + c_{12}\alpha_1 + c_{13}\alpha_3)$  and  $\gamma_3 = \frac{1}{C}(2c_{13}\alpha_1 + c_{33}\alpha_3)$  [6], and  $\Sigma''$  reduces to  $\Sigma'' = d_{33}\gamma_3C$  for a clamped film.  $\Sigma''$  has the opposite sign as  $\Sigma'$  ( $\Sigma' < 0$ ;  $\Sigma'' > 0$ ): with increasing electric fields the PZT layers expand and, due to anharmonicity, the vibrational frequencies of the lattice are reduced. This softening of the lattice vibrations increases the vibrational entropy [5,7]. On the other hand, an increasing field lowers the entropy of the system associated with the polarization by the primary electrocaloric effect. These opposing mechanisms reduce the overall entropy change that is achievable.

The thermodynamic Maxwell relation shows that the pyroelectric and electrocaloric coefficients are equal at constant strain or stress condition (see eq. 35 of Ref. [8]):

$$\begin{aligned} \Pi' &= \Sigma' \\ \Pi|_{\sigma} &= \Sigma|_{\sigma}. \end{aligned} \quad (5)$$

Hence, the secondary pyroelectric and electrocaloric coefficient are equal,  $\Pi'' = \Sigma''$  under constant stress condition.

\*trongvantong@gmail.com; tong16@illinois.edu

The derivations of  $\Pi''$  and  $\Sigma''$  for tetragonal symmetry case (Eqs. (2) and (4)) agree with this result because the direct and converse piezoelectric coefficients are equal (eq. (2) of Ref [9]). This relation is the basis of the so-called ‘‘indirect’’ method to study the electrocaloric effect both theoretically and experimentally [10–15].

However, for clamped films, the difference between the total electrocaloric coefficient and the total pyroelectric coefficient is  $\Sigma - \Pi = \Sigma'' - \Pi'' = d_{33}\gamma_3 C - d_{33}^* c_{33} \alpha_3$ . Both the direct and converse piezoelectric coefficients (the so-called effective coefficients) are both reduced by a factor of  $\sim 2$  compared to an unclamped film [4]. The calculation by Lefki and Dormans [4] shows that the effective direct piezoelectric coefficient is larger than the effective converse one (see eqs. (2) and (3) of Ref. [4]) because of a contribution from the mechanical deformation of the substrate. However, in our measurement the substrate is fixed so that  $d_{33}^* = d_{33}$ . Therefore, we simplify the equation for  $\Sigma - \Pi$  as

$$\Sigma - \Pi = d_{33}(\gamma_3 C - c_{33}\alpha_3) = 2d_{33}c_{13}\alpha_1. \quad (6)$$

Thus, a measurement of the difference between the total coefficients captures the first term in the following expression for the secondary electrocaloric coefficient,  $\Sigma'' = d_{33}\alpha_1(2c_{13} + c_{33})$ , where we have set  $\alpha_1 = \alpha_3$ . For PZT,  $c_{13} = 68$  GPa,  $c_{33} = 113$  GPa [16], and  $\alpha_1 = 5.4 \times 10^{-6} \text{ K}^{-1}$  [17]. Since  $2c_{13} \approx c_{33}$ ,  $\Sigma'' \approx 2(\Sigma - \Pi)$ .

In this paper, we use two novel laser-based methods to independently measure the total pyroelectric ( $\Pi$ ) and electrocaloric coefficients ( $\Sigma$ ) of PZT epitaxial layers. Because our measurements are performed with high-frequency thermal fields, the mechanical conditions of our electrocaloric measurements are the same as for the pyroelectric measurements; i.e., the in-plane strain is zero. Combining these methods allows us to quantify the secondary contribution to the total electrocaloric coefficient. We find that the secondary electrocaloric effect significantly reduces the total electrocaloric response and should be considered in evaluating the performance of electrocaloric materials and heat engines.

## II. EXPERIMENT

Capacitor structures are fabricated from heterostructures of 20 nm SrRuO<sub>3</sub>/150 nm PZT/20 nm SrRuO<sub>3</sub> grown on DyScO<sub>3</sub> (DSO) (110) and GdScO<sub>3</sub> (GSO) (110) substrates

by pulsed-laser deposition (see the Appendix, Sample Preparation). We use PZT layers as the subject of our study because deposition conditions and lattice structures are well established [18]. SrRuO<sub>3</sub> (SRO) is used as top and bottom electrodes because of its good metallic conductivity and lattice matching with perovskite substrates. These capacitor structures enable us to apply electric fields in the electrocaloric measurement and collect the pyroelectric current in the pyroelectric measurement. Circular SRO top electrodes with a radius of 50  $\mu\text{m}$  or 100  $\mu\text{m}$  are patterned by photolithography utilizing a MgO hard-mask process [19]. We prepared and measured three samples: two compositionally homogenous PbZr<sub>0.2</sub>Ti<sub>0.8</sub>O<sub>3</sub> (PZT20:80) epitaxial layers on DSO and GSO substrates and one compositionally graded heterostructure that smoothly transitions from PbZr<sub>0.2</sub>Ti<sub>0.8</sub>O<sub>3</sub> to PbZr<sub>0.8</sub>Ti<sub>0.2</sub>O<sub>3</sub> from the GSO substrate to the surface (graded PZT) [20]. Vanadium (V) films  $\approx 150$  nm thick are sputtered on top of the SRO top electrodes to produce an optical transducer that absorbs the incident laser power and provides a strongly temperature dependent optical reflectivity, i.e., a high thermoreflectance, for measurements of the electrocaloric coefficient [21].

Thermal conductivities of each layer and the thermoreflectance coefficients of the V film are measured by time domain thermoreflectance (TDTR) [7]. The thickness of the V film is measured by picosecond acoustics [22]. These properties are used as input parameters of thermal transport models for the pyroelectric and electrocaloric measurement (see Appendix, Table I).

The pyroelectric coefficient is measured by the laser intensity modulation method [see Appendix Fig. 7(a)] [23]. A mode-locked Ti:sapphire laser operating at a wavelength of 785 nm is modulated in the frequency range of 10 kHz to 10 MHz by an electro-optic modulator and focused on the surface of the V film by a  $5 \times$  objective lens. The  $1/e^2$  intensity radius of the focused laser spot is  $\approx 10 \mu\text{m}$ . The laser power absorbed by the V film produces an oscillating temperature within the ferroelectric layer and substrate. To minimize the steady-state temperature rise, the average laser power is chosen to be 1 mW, which creates a  $\sim 5$  K steady-state temperature rise. A lock-in amplifier synchronized to the laser modulation measures the current generated by charges that compensate for the change of polarization of the ferroelectric layer created by the pyroelectric effect.

TABLE I. Thermophysical properties of PZT, DSO, GSO, SRO, and V measured by TDTR and from literatures used in the thermal transport calculation.

	25 (°C)	75 (°C)	150 (°C)	220 (°C)
$C_{\text{PZT}}$ ( $\text{J m}^{-3} \text{K}^{-1}$ ) <sup>a</sup>	$2.7 \times 10^6$	$2.9 \times 10^6$	$3.1 \times 10^6$	$3.2 \times 10^6$
$\Lambda_{\text{PZT}}$ ( $\text{W m}^{-1} \text{K}^{-1}$ )	1.5	1.5	1.5	1.5
$C_{\text{SRO}}$ ( $\text{J m}^{-3} \text{K}^{-1}$ ) <sup>b</sup>	$3.00 \times 10^6$	$3.1 \times 10^6$	$3.17 \times 10^6$	$3.24 \times 10^6$
$\Lambda_{\text{SRO}}$ ( $\text{W m}^{-1} \text{K}^{-1}$ )	3.9	3.9	3.9	3.9
$C_{\text{DSO}} \times \Lambda_{\text{DSO}}$ ( $\text{J W m}^{-4} \text{K}^{-2}$ )	$7.3 \times 10^6$	$7.3 \times 10^6$	$7.3 \times 10^6$	$7.3 \times 10^6$
$C_{\text{GSO}} \times \Lambda_{\text{GSO}}$ ( $\text{J W m}^{-4} \text{K}^{-2}$ )	$7.3 \times 10^6$	$7.3 \times 10^6$	$7.3 \times 10^6$	$7.3 \times 10^6$
$C_V$ ( $\text{J m}^{-3} \text{K}^{-1}$ ) <sup>c</sup>	$2.95 \times 10^6$	$2.97 \times 10^6$	$3.0 \times 10^6$	$3.06 \times 10^6$
$\Lambda_V$ ( $\text{W m}^{-1} \text{K}^{-1}$ )	21	21	21	21

<sup>a</sup>Ref. [39].

<sup>b</sup>Ref. [40].

<sup>c</sup>Ref. [41].

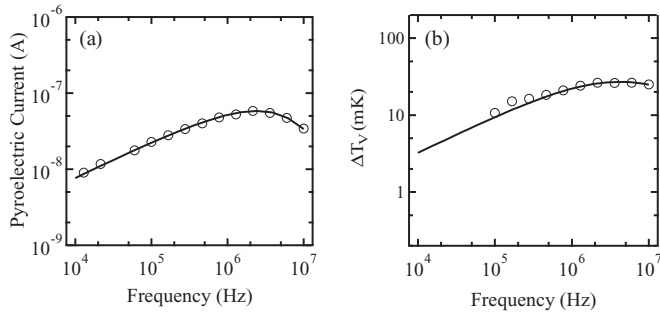


FIG. 1. (a) Frequency dependence of the pyroelectric current and (b) frequency dependence of the temperature change of the V film for a PZT/GSO capacitor at room temperature. Measured data are shown as open circles, and the solid lines are the model calculations used to determine (a) the total pyroelectric coefficient  $\Pi = -170 \mu\text{C m}^{-2} \text{K}^{-1}$  and (b) the total electrocaloric coefficient  $\Sigma = -130 \mu\text{C m}^{-2} \text{K}^{-1}$ . The laser power used in the pyroelectric measurement is 1 mW. The dc bias voltage and ac voltage used in the electrocaloric measurement are 1.4 V and 1 V, respectively.

The temperature oscillation,  $T(f, r, z)$ , within the ferroelectric epitaxial layers is calculated by a multilayer thermal transport model [7] in cylindrical coordinates (see Appendix, Pyroelectric Measurement). Here,  $f$  is the modulation frequency,  $r$  is the radial coordinate, and  $z$  is the out-of-plane coordinate. The measured pyroelectric current is related to the temperature oscillation by:

$$I(f) = 2\pi f \frac{1}{h} \Pi \int_0^a \int_0^h T(f, r, z) 2\pi r dr dz. \quad (7)$$

Here,  $a$  is the radius of the top electrode of the capacitors, and  $h$  is the thickness of the ferroelectric layer. Figure 1(a) shows the dependence of the pyroelectric current for a PZT/GSO capacitor on modulation frequency. The pyroelectric coefficient is adjusted to get the best fit between the measured current and the model calculation. We find  $\Pi = -170 \mu\text{C m}^{-2} \text{K}^{-1}$ .

The direct electrocaloric measurement is carried out by applying a sinusoidal voltage to the same capacitor to produce sinusoidal electric fields within the ferroelectric layer, which result in temperature changes,  $\Delta T$  [see Appendix Fig. 5(a)]. The temperature changes are measured through changes of the optical reflectivity of the V films by monitoring the intensity change of a laser beam reflected from the V films. The reflected laser beam is focused on a photodiode connected to an rf lock-in amplifier to detect the signal synchronously with the applied voltage.

The heat flux created by the entropy change has the form

$$F = T \frac{dS}{dT} \frac{dE}{dT} = T \Sigma E_0 2\pi f e^{-i2\pi ft}. \quad (8)$$

Here,  $T$  is the ambient temperature,  $E_0$  is the amplitude of the oscillating electric field applied to the capacitors,  $f$  is the frequency of the oscillating electric field, and  $\Sigma$  is the total electrocaloric coefficient. In our experiment, we select the reasonable low value of  $E_0$  as a trade-off between signal-to-noise and linearity of the response. High frequencies are required to achieve high heat flux to produce a significant temperature change. In our electrocaloric measurement, the frequency range is 100 kHz to 10 MHz. The electrocaloric

coefficient is determined by the heat flux, which can be calculated with the knowledge of the measured temperature change at the V films and the thermal properties of each layer (see Appendix, Electrocaloric Measurement and Eq. (A2)). Since the electrode radius ( $50 \mu\text{m}$ ) is much larger than the thermal penetration depth,  $d = \sqrt{\Lambda/(\pi f C)} = 0.2\text{--}2 \mu\text{m}$ , heat transport is approximately one dimensional. The generated heat flux is uniform within the ferroelectric layer and diffuses in both directions, i.e., into the substrate and into the V film. A bidirectional heat flow model [24] is used to take into account the heat flux distribution over the ferroelectric layers.

Figure 1(b) shows the dependence of the temperature change of the V film as a function of frequency for a PZT20:80/GSO capacitor. A dc bias voltage of 1.4 V is applied on the capacitor along with the ac voltage of amplitude of 1 V to produce a voltage that varies from 0.4 V to 2.4 V. (We determined empirically that the range of linearity extends to an ac voltage of amplitude 1 V.) The dc voltage is chosen to make sure that the ferroelectric layers do not switch polarization states under applied voltages. As shown below, by varying the dc bias voltage, we probe the hysteresis behavior of the electrocaloric coefficient. Adjusting the electrocaloric coefficient to get the best fit between the experimental data and the modeling calculation yields  $\Sigma = -130 \mu\text{C m}^{-2} \text{K}^{-1}$  for the PZT20:80 epitaxial layer on the GSO substrate. The adiabatic electrocaloric temperature change within the PZT layer is calculated as

$$\Delta T_a = -\frac{1}{C} T \frac{dS}{dE} \Delta E. \quad (9)$$

Using the measured electrocaloric coefficient  $dS/dE = \Sigma = -130 \mu\text{C m}^{-2} \text{K}^{-1}$ ,  $\Delta T_a \approx 0.1 \text{K}$  for a field change of  $6.7 \text{MV m}^{-1}$ . We emphasize that our electrocaloric method measures the total heat generated within the PZT layers through measuring the temperature change of the V film. The measured temperature change plotted in Fig. 1(b) is much smaller than the adiabatic temperature change, i.e., the temperature change of the PZT layer if the PZT layer was thermally isolated from the V film and substrate. While wires and contact tips needed to drive the electrocaloric effect are present, it does not affect the temperature measurement because of high modulation frequencies of the electric field.

The errors in our measurements depend largely on the uncertainties in the measurement of the laser power,  $\approx 5\%$ , and uncertainties of the thermophysical properties of the materials in the capacitor structure, typically  $\approx 10\%$ . The sensitivity of the measurement to the various experimental parameters, i.e., the error propagation, is discussed in the Appendix (Fig. 8). Propagation of errors from the thermophysical properties to the pyroelectric and electrocaloric data is similar; the propagation of errors from the laser power, however, has the opposite sign. Therefore, the uncertainty in the difference between the pyroelectric and electrocaloric data is relatively insensitive to uncertainties in the thermophysical properties and mostly depends on the uncertainty in the measurement of the laser power. As a specific example, we estimate that measurements summarized by Fig. 1 have total uncertainties of 10%, i.e.,  $\Pi = -170 \pm 17 \mu\text{C m}^{-2} \text{K}^{-1}$  and  $\Sigma = -130 \pm 13 \mu\text{C m}^{-2} \text{K}^{-1}$ , while the uncertainty in the difference,  $\Pi - \Sigma = -40 \pm 15 \mu\text{C m}^{-2} \text{K}^{-1}$  is given by the

sum of the contribution of the uncertainty of the laser power to the uncertainty in each measurement.

In our measurement, the detector is at an image of the sample surface so a small translation of the sample surface does not change the reflectivity. Another factor that could affect the optical reflectivity of the V films is strain. However, the lateral strain of V film is zero at high frequencies. Joule heating by the leakage currents under dc bias has no effect on the electrocaloric measurement because the look-in amplifier only picks up the temperature changes that are synchronous with the modulation frequency of the electric field while the Joule heating is at double the modulation frequency.

We noted that in our electrocaloric and pyroelectric measurement, PZT layers are clamped on the fixed substrates. For the pyroelectric measurement, because of high modulation frequency of the heating laser (100 kHz–10 Mhz), heat is confined laterally. Therefore, there is no in-plane contraction of the substrate, and the PZT layers only contract in the out-of-plane direction. For the electrocaloric measurement, because the radius of the devices is very small compared to the size of the samples, the PZT layers only contract in the out-of-plane direction due to the converse piezoelectric effect.

### III. RESULTS

To directly compare the pyroelectric and electrocaloric coefficients, the two coefficients must be measured at the same bias field. Therefore, we measure the pyroelectric and electrocaloric coefficient as a function of dc bias voltage. For all three samples, our result shows that the pyroelectric and electrocaloric coefficient are not equal at the same field. Furthermore, the pyroelectric and electrocaloric coefficients show hysteresis that is consistent with the polarization measurement (Fig. 2). The hysteresis curves for the polarization and the pyroelectric and electrocaloric coefficient are shifted horizontally. This shift could arise from slight differences in the top and bottom contacts, trapped charges for the homoge-

neous PZT layer, and the presence of strain gradients for the compositionally graded PZT layer [20,25–27]. The coercive voltages in the pyroelectric measurement are smaller than the corresponding coercive voltages in the polarization measurement. This difference is explained by the fact that the bias voltage in the pyroelectric and electrocaloric measurement is changed slowly, with  $\sim 30$  second intervals between each value of the bias voltage, while the polarization is measured at 1 kHz.

Furthermore, the electrocaloric hysteresis loops are even narrower than the pyroelectric curves. A smaller dc voltage is required to switch polarization in the electrocaloric measurement than the pyroelectric measurement because of the additional ac voltage used in the electrocaloric measurement. The pyroelectric and electrocaloric coefficients are independent of the dc voltage up to 3 V.

The field dependence of the electrocaloric effect has been studied previously for bulk materials [28–31]. However, in the prior work reported in Refs. [29–32], the adiabatic temperature changes are measured as a function of the change in electric field ( $\Delta E = E_2 - E_1$ , and  $E_1$  is often chosen to be 0). For our measurement of the electric-field dependence, the amplitude of oscillating electric field that drives the electrocaloric effect,  $\Delta E$ , is fixed, and the dc bias voltage slowly varied from point to point. Since the adiabatic temperature change depends not only on  $\Delta E$  but also on the polarization state, our measurement provides a more complete picture of how the entropy changes with a small variation in electric field.

Our key result is that the measured electrocaloric and pyroelectric coefficients are not equal. If we calculate the adiabatic temperature change using the field dependence of the measured pyroelectric coefficient predicted and the Maxwell relation,  $\Delta T_a = -\frac{T}{C} \int_{E_1}^{E_2} \left(\frac{dP}{dT}\right)_E dE = -\frac{T}{C} \int_{E_1}^{E_2} \Pi(E) dE$ , we find  $\Delta T_a \approx 0.14$  K for  $\Delta E = 6.7$  MV m $^{-1}$  for the PZT20:80/DSO layer. This indirect measurement of the adiabatic temperature change is 40% higher than the value obtained by the direct measurement, 0.10 K. Note that while the conventional indirect method for the electrocaloric measurement extracts  $dP/dT$  from the temperature dependence of the polarization at a different field [10], our pyroelectric measurement directly measures the dependence of  $dP/dT$  on the electric field.

To further probe the differences between  $\Sigma$  and  $\Pi$ , we measured the pyroelectric and electrocaloric coefficients as a function of temperature from room temperature to 220 °C for the three PZT epitaxial layers (Fig. 3). The pyroelectric coefficient (square symbols) increases with elevated temperature for all samples, while the electrocaloric coefficient (triangles) has a weaker dependence on temperature. The graded PZT

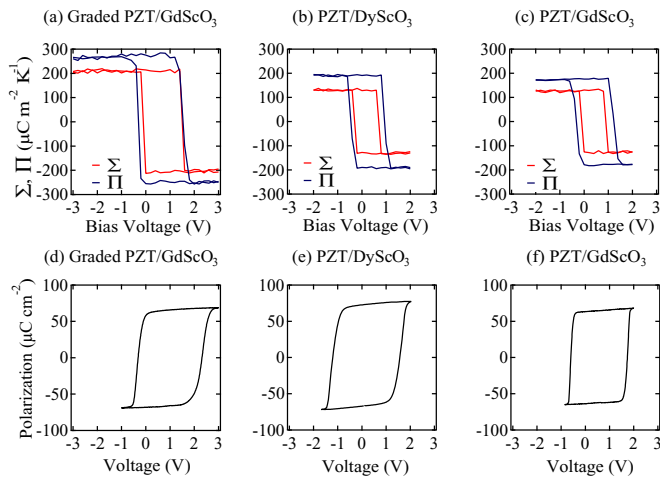


FIG. 2. (Color online) Hysteresis measurement of the total pyroelectric, electrocaloric coefficient, and polarization of the PZT layers at room temperature. For the electrocaloric and pyroelectric measurements, a dc bias voltage is applied to the capacitors, and the time between changes in the bias voltage is  $\sim 30$  s with an increment of 0.1 V. Polarization is measured at a frequency of 1 kHz.

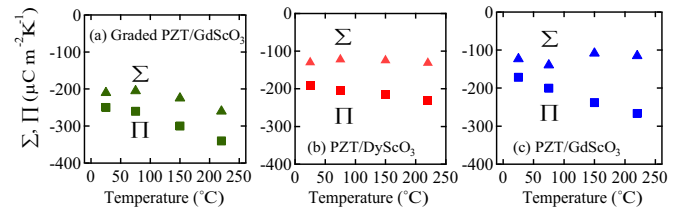


FIG. 3. (Color online) Dependence on sample temperature of the total electrocaloric (triangle symbols) and pyroelectric (square symbols) coefficients of PZT epitaxial layers on DyScO $_3$  and GdScO $_3$  substrates.

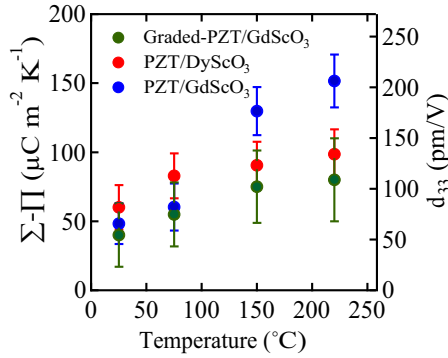


FIG. 4. (Color online) Temperature dependence of the *difference* between the total electrocaloric coefficient and pyroelectric coefficient of PZT epitaxial layers due to the secondary contribution. The converse piezoelectric coefficient  $d_{33}$  calculated based on Eq. (6). The error bar is calculated with uncertainties of the pyroelectric and electrocaloric measurement to be 5%.

layer has a higher pyroelectric coefficient and electrocaloric coefficient than the homogeneous layers.

Our data are in qualitative agreement with the result from Ref. [11]. In Ref. [11], the temperature change measured by the direct method is smaller than the temperature change inferred by the indirect method. The difference increases from  $\sim 10\%$  at the room temperature to  $\sim 40\%$  at  $\sim 340$  K and then decreases with further increases in temperature.

Figure 4 shows the difference between the total pyroelectric and electrocaloric coefficients. The corresponding value of  $d_{33}$  using Eq. (6) is plotted as the right-hand axis in Fig. 4. The values of  $d_{33}$  fall in the same range with those reported for PZT layers [32,33]. We see that  $d_{33}$  increases with increasing temperature for all samples, consistent with previous studies of PZT epitaxial layers [34] and LiTaO<sub>3</sub> crystals [35].

At high temperatures, the secondary electrocaloric coefficient by piezoelectric strain and the elastocaloric effect is comparable to the primary coefficient. For example, for the PZT20:80/GSO sample at 200 °C,  $\Sigma \approx -100 \mu\text{C m}^{-2} \text{K}^{-1}$ ;  $\Sigma - \Pi \approx 150 \mu\text{C m}^{-2} \text{K}^{-1}$ ; and, therefore,  $\Sigma' \approx -400 \mu\text{C m}^{-2} \text{K}^{-1}$  and  $\Sigma'' \approx 300 \mu\text{C m}^{-2} \text{K}^{-1}$ .

Large elastocaloric effects have been found in shape-memory alloys [36] and predicted theoretically for Ba<sub>0.5</sub>Sr<sub>0.5</sub>TiO<sub>3</sub> (BST) [37]. A temperature change of  $\sim 9$  K is estimated for BST with a strain of 0.008. Lisenkov and Ponomareva [37] attributed this giant elastocaloric effect of BST to a stress-induced ferroelectric structural phase transition. For a qualitative comparison, using Eq. (9), we estimate a temperature change  $\sim 1.5$  K under the same strain for our PZT layers. While the stand-alone elastocaloric effect can be comparable to the electrocaloric effect, our data shows that elastocaloric effect induced by piezoelectric effect competes with the electrocaloric effect for typical ferroelectric materials.

#### IV. CONCLUSION

We anticipate that our methods for studying the electrocaloric and pyroelectric effect in thin epitaxial layers will provide insights on caloric effects in pyroelectric and ferroelectric materials. These methods overcome experimental

limitations of previous techniques that restricted widespread study of caloric effects in thin layers. Our results show that secondary, mechanical effects produce a significant contribution to the entropy change for clamped films

#### ACKNOWLEDGMENTS

The study of electrocaloric effects and materials was supported by the Air Force Office of Scientific Research under Grant No. AF FA 9550-11-1-0073. The study of pyroelectric effects and materials was supported by the Office of Naval Research under Grant No. N00014-10-10525. The development of compositionally graded pyroelectric/electrocaloric layers was supported by the Defense Advanced Research Projects Agency (DARPA) under Grant No. N66001-11-1-4195 and the Army Research Office under Grant No. W911NF-10-1-0482. Experiments were carried out, in part, in the Materials Research Laboratory Central Facilities, University of Illinois, Urbana-Champaign.

#### APPENDIX

##### 1. Sample preparation

The SRO and PbZr<sub>1-x</sub>Ti<sub>x</sub>O<sub>3</sub> layers were fabricated by pulsed-laser deposition employing a KrF excimer laser (wavelength = 248 nm). Ceramic SRO, Pb<sub>1.1</sub>Zr<sub>0.2</sub>Ti<sub>0.8</sub>O<sub>3</sub>, and Pb<sub>1.1</sub>Zr<sub>0.8</sub>Ti<sub>0.2</sub>O<sub>3</sub> targets (Praxair Specialty Ceramics) were used for the growth. The SRO layer (thickness = 20 nm) was deposited at 630 °C in an oxygen pressure of 100 mTorr with a laser fluence of 1.75 J/cm<sup>2</sup> at a laser repetition rate of 12 Hz. Compositionally homogeneous single-layer PbZr<sub>0.2</sub>Ti<sub>0.8</sub>O<sub>3</sub> films (thickness = 150 nm) were grown from PZT targets with the same composition at 630 °C in an oxygen pressure of 200 mTorr at a laser fluence of 2 J/cm<sup>2</sup> and a laser repetition rate of 3 Hz. Compositionally graded heterostructures (thickness = 150 nm) were synthesized from Pb<sub>1.1</sub>Zr<sub>0.2</sub>Ti<sub>0.8</sub>O<sub>3</sub> and Pb<sub>1.1</sub>Zr<sub>0.8</sub>Ti<sub>0.2</sub>O<sub>3</sub> targets at 600 °C at a laser fluence of 1.9 J/cm<sup>2</sup> in 200 mTorr of oxygen and a laser repetition rate of 3 Hz. Compositionally graded heterostructures were synthesized by continuously varying the composition from PbZr<sub>0.2</sub>Ti<sub>0.8</sub>O<sub>3</sub> to PbZr<sub>0.8</sub>Ti<sub>0.2</sub>O<sub>3</sub> using a programmable target rotator (Neocera, LLC) that was synced with the excimer laser. After growth, all the samples were cooled in 700 Torr pressure of oxygen to room temperature at 5 K/min. The thickness of the films is determined by deposition time and rate, which is calibrated for each material.

##### 2. Electrocaloric measurement

Figure 5(a) shows a schematic of the electrocaloric measurement. The temperature changes of the V film are determined from Ref. [7]:

$$\Delta T(t) = \frac{\sqrt{2}}{G} \frac{V(t)}{V_0} \frac{dT}{dR} R. \quad (\text{A1})$$

Here,  $R$  is the reflectivity of the V film,  $dR/dT$  is the thermorefectance coefficient,  $V(t)$  is the voltage signal measured by the lock-in amplifier,  $V_0$  is the average dc voltage generated by the photodiode, and  $G$  is the gain of the pre amplifier.  $V$  is chosen as the thermal transducer because it has a large

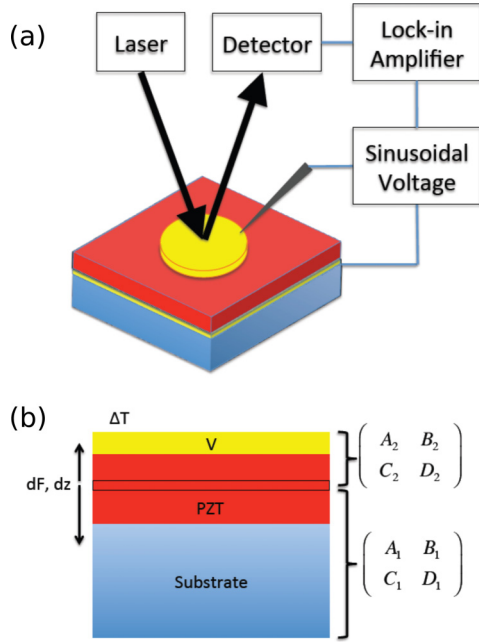


FIG. 5. (Color online) (a) The schematic of the electrocaloric measurement. (b) Thermal model for bidirectional heat conduction into the V film and substrate.

value of  $(1/R)(dR/dT)$  at the wavelength of 785 nm [21]. We measure  $dR/dT \approx 0.79 \times 10^{-4} \text{ K}^{-1}$ , which agrees with the reported data ( $0.76 \times 10^{-4} \text{ K}^{-1}$ ) [21].

We confirm the accuracy of the measurement of  $dR/dT$  by using a 2-omega method (see Fig. 6). A metal pattern (A1) is produced by a photolithography through a mask on a  $\text{SiO}_2$  substrate. A sinusoidal voltage is applied on the metal line to produce an oscillating temperature at a frequency of two times of a source frequency. A laser beam is used to probe the temperature change through the change of the thermal reflectivity of the metal line. By using a thermal model [38], the temperature change of the metal line is calculated and then  $dR/dT$  is extracted through Eq. (A1). The  $dR/dT$  measured by the 2-omega method ( $dR/dT \approx 0.81 \times 10^{-4} \text{ K}^{-1}$ ) and the TDTR method are in good agreement with each other.

To solve the heat transport problem with the heat generated uniformly within the ferroelectric films, we solve the one-dimensional problem for a heat flux generated in a thin slab of

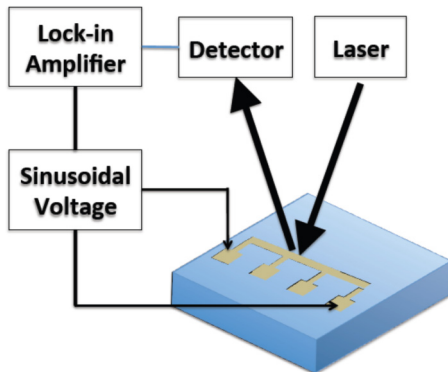


FIG. 6. (Color online) A schematic of the 2-omega method to measure the thermorefectance coefficient.

ferroelectric film,  $dF = F dz$  [see Fig. 5(b)], and then sum the contributions from all slabs. For each slab, the heat  $dF$  diffuses to the substrate and the V film. We define multiple layers from the slab to the substrate to be system 1 (PZT/SRO/substrate) and from the slab to the V film to be system 2 (PZT/SRO/V). Each system is described by a transport matrix, which is a multiplication of matrices of individual layers (see eqs. (3) and (4) of Ref. [24]). Solving the heat transport problem corresponding to the heat flux  $dF$  and taking integral over the thickness of the ferroelectric film give the temperature change at the V film surface relating to the heat flux  $F$

$$\Delta T = \int_0^h \left( \frac{B_2 C_2 - A_2 D_2}{D_1 C_2 + C_1 D_2} D_1 \right) F dz. \quad (\text{A2})$$

Here,  $D_1$ ,  $C_1$  and  $A_2$ ,  $B_2$ ,  $C_2$ ,  $D_2$  are the matrix elements corresponding to system 1 and system 2.

### 3. Pyroelectric measurement

Figure 7(a) shows the schematic of the pyroelectric measurement. To solve the temperature change,  $T(f, r, z)$ , we calculate matrices for multiple layers of the sample (five layers: V/SRO/PZT/SRO/substrate),  $\begin{pmatrix} A & B \\ C & D \end{pmatrix}$  and multiple layers from  $z$  to the V surface (three layers: V/SRO/PZT),  $\begin{pmatrix} A_z & B_z \\ C_z & D_z \end{pmatrix}$  [Fig. 7(b)]. The temperature change at the V surface,  $T_V$ , relates to the heat flux created by a laser,  $F$  by (see eq. (5) of Ref. [24])

$$T_V = -\frac{D}{C} F. \quad (\text{A3})$$

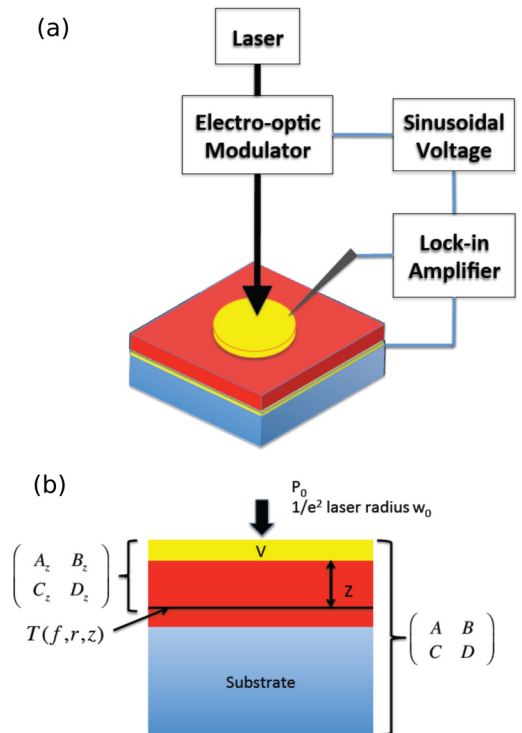


FIG. 7. (Color online) (a) The schematic of the pyroelectric measurement. (b) The heat transport model for the pyroelectric measurement

The temperature change within the ferroelectric layer,  $T(f, r, z)$  in  $k$  space relates to  $T_V$  by the following equation:

$$T(f, r, z) = A_z T_V + B_z F = \left( -A_z \frac{D}{C} + B_z \right) F. \quad (\text{A4})$$

The final solution for  $T(f, r, z)$  in real space is given by

$$T(f, r, z) = \frac{P_0}{2\pi} \int_0^\infty \left( -A_z \frac{D}{C} + B_z \right) k J_0(kr) \times \exp\left(-\frac{k^2 w_0^2}{8}\right) dk. \quad (\text{A5})$$

Here,  $J_0(kr)$  is the zero-order Bessel function.

#### 4. Sensitivity of the electrocaloric and pyroelectric measurement to the thermophysical properties

The sensitivity of the electrocaloric and pyroelectric measurement is defined by

$$S_\alpha = \frac{\partial \ln T}{\partial \ln \alpha}. \quad (\text{A6})$$

Here  $T$  is the averaging temperature change within the PZT layers in the pyroelectric measurement and the temperature change of V films in the electrocaloric measurement.  $\alpha$  is one of the parameters (thermal conductivity  $\Lambda$ , heat capacity  $C$ , and thickness  $h$ ). Figure 8 shows the sensitivity to the thermophysical properties of PZT, DSO and V as a function of frequencies.

#### 5. Suppression of the signal at high frequencies by capacitance of the system

At high frequencies ( $f > 5$  MHz) at which the capacitance of the device and cables are comparable to the input impedance of the lock-in amplifier used in the pyroelectric measurement or the output impedance of the voltage source used in the electrocaloric measurement, the signal will be suppressed by a factor  $1/(iRC\omega + 1)$ . Here,  $R$  is the input or output impedance, and  $C$  is equivalent capacitor of the device and

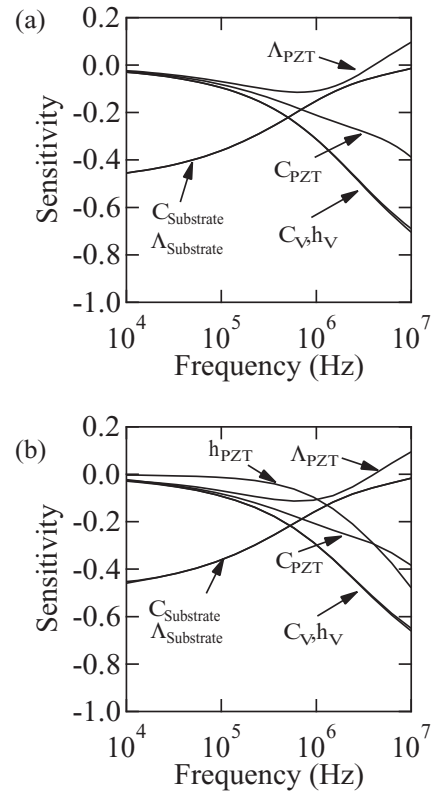


FIG. 8. Sensitivity of the electrocaloric measurement (a) and the pyroelectric measurement (b) to the thermophysical properties of PZT, DSO, and V as a function of frequencies. Sensitivity to the laser power is 1. Sensitivity to the thickness of the PZT films in the electrocaloric measurement is 0.

cables. We adjust  $C$  to have the best fit at high frequencies. We found values of  $C$  to be in the range of 300–400 pF. For our measurement, capacitances of the devices is in order of 100 pF and total BNC cable length is  $\sim 2$  to 3 m, which creates a capacitance of  $\sim 200$ –300 pF.

- 
- [1] J. Scott, *Annu. Rev. Mater. Res.* **41**, 229 (2011).  
 [2] S. Fähler, U. K. Rößler, O. Kastner, J. Eckert, G. Eggeler, H. Emmerich, P. Entel, S. Müller, E. Quandt, and K. Albe, *Advanced Engineering Materials* **14**, 10 (2012).  
 [3] S. B. Lang, *Nature* **224**, 798 (1969).  
 [4] K. Lefki and G. J. M. Dormans, *J. Appl. Phys.* **76**, 1764 (1994).  
 [5] S. Boffi, G. Caglioti, and G. Cortellazzi, *J. Phys. Chem. Solids* **39**, 5 (1978).  
 [6] S. W. Key, *J. Appl. Phys.* **38**, 2923 (1967).  
 [7] D. Cahill, *Rev. Sci. Instrum.* **75**, 5119 (2004).  
 [8] R. W. Munn, *J. Phys. C: Solid State Physics* **6**, 3213 (1973).  
 [9] S. V. Kalinin, B. Mirman, and E. Karapetian, *Phys. Rev. B* **76**, 212102 (2007).  
 [10] A. Mischenko, Q. Zhang, J. Scott, R. Whatmore, and N. Mathur, *Science* **311**, 1270 (2006).  
 [11] S. Kar-Narayan and N. Mathur, *J. Phys. D Appl Phys* **43**, 032002 (2010).  
 [12] S. G. Lu, B. Rožič, Q. M. Zhang, Z. Kutnjak, X. Li, E. Furman, L. J. Gorny, M. Lin, B. Malič, M. Kosec, R. Blinc, and R. Pirc, *Appl. Phys. Lett.* **97**, 162904 (2010).  
 [13] Y. Bai, G. Zheng, and S. Shi, *Appl. Phys. Lett.* **96**, 192902 (2010).  
 [14] F. L. Goupil, A. Berenov, A.-K. Axelsson, M. Valant, and N. M. Alford, *J. Appl Phys* **111**, 124109 (2012).  
 [15] I. I. Ponomareva and S. S. Lisenkov, *Phys. Rev. Lett.* **108**, 167604 (2012).  
 [16] Y.-Z. Chen, T.-H. Liu, C.-Y. Chen, C.-H. Liu, S.-Y. Chen, W.-W. Wu, Z. L. Wang, J.-H. He, Y.-H. Chu, and Y.-L. Chueh, *Acs Nano* **6**, 2826 (2012).  
 [17] J. Karthik and L. W. Martin, *Phys. Rev. B* **84**, 024102 (2011).

- [18] N. Izyumskaya, Y. Alivov, S. J. Cho, H. Morkoc, H. Lee, and Y. S. Kang, *Critical Revs. in Solid State & Mat. Sc.* **32**, 111 (2007).
- [19] J. Karthik, A. R. Damodaran, and L. W. Martin, *Adv. Mater. Weinheim* **24**, 1610 (2012).
- [20] R. V. K. Mangalam, J. Karthik, A. R. Damodaran, J. C. Agar, and L. W. Martin, *Adv. Mater.* **25**, 1761 (2013).
- [21] Y. Wang, J. Y. Park, Y. K. Koh, and D. G. Cahill, *J. Appl. Phys.* **108**, 043507 (2010).
- [22] W. S. Capinski, H. J. Maris, T. Ruf, M. Cardona, K. Ploog, and D. S. Katzer, *Phys. Rev. B* **59**, 8105 (1999).
- [23] S. B. Lang and D. K. Das-Gupta, *Ferroelectrics* **60**, 23 (1984).
- [24] A. Schmidt, M. Chiesa, X. Chen, and G. Chen, *Rev. Sci. Instrum.* **79**, 064902 (2008).
- [25] J. Karthik, R. V. K. Mangalam, J. C. Agar, and L. W. Martin, *Phys. Rev. B* **87**, 024111 (2013).
- [26] M. Grossmann, O. Lohse, D. Bolten, U. Boettger, T. Schneller, and R. Waser, *J. Appl. Phys.* **92**, 2680 (2002).
- [27] M. B. Okatan and S. P. Alpay, *Appl. Phys. Lett.* **95**, 092902 (2009).
- [28] L. J. Dunne, M. Valant, G. Manos, A.-K. Axelsson, and N. Alford, *Appl. Phys. Lett.* **93**, 122906 (2008).
- [29] M. Valant, L. J. Dunne, A.-K. Axelsson, N. McN. Alford, G. Manos, J. Peräntie, J. Hagberg, H. Jantunen, and A. Dabkowski, *Phys. Rev. B* **81**, 214110 (2010).
- [30] J. Hagberg, A. Uusimaki, and H. Jantunen, *Appl. Phys. Lett.* **92**, 132909 (2008).
- [31] G. Akcay, S. P. Alpay, J. V. Mantese, and G. A. Rossetti, *Appl. Phys. Lett.* **90**, 252909 (2007).
- [32] V. Nagarajan, A. Stanishevsky, L. Chen, T. Zhao, B. T. Liu, J. Melngailis, A. L. Roytburd, R. Ramesh, J. Finder, Z. Yu, R. Droopad, and K. Eisenbeiser, *Appl. Phys. Lett.* **81**, 4215 (2002).
- [33] D. V. Taylor and D. Damjanovic, *Appl. Phys. Lett.* **76**, 1615 (2000).
- [34] B. Bhatia, J. Karthik, D. G. Cahill, L. W. Martin, and W. P. King, *Appl. Phys. Lett.* **99**, 173103 (2011).
- [35] T. Yamada, H. Iwasaki, and N. Niizeki, *Japanese J. Applied Physics* **8**, 1127 (1969).
- [36] E. E. Bonnot, R. R. Romero, L. L. Mañosa, E. E. Vives, and A. A. Planes, *Phys. Rev. Lett.* **100**, 125901 (2008).
- [37] S. Lisenkov and I. Ponomareva, *Phys Rev B* **86**, 104103 (2012).
- [38] D. G. Cahill, *Rev. Sci. Instrum.* **61**, 802 (1990).
- [39] G. Suchaneck, G. Gerlach, A. Deyneka, L. Jastrabik, S. T. Davitadze, and B. A. Strukov, *Mat. Res. Soc. Proc.* **718**, D8.4.1 (2002).
- [40] S. Yamanaka, T. Maekawa, H. Muta, T. Matsuda, S.-I. Kobayashi, and K. Kurosaki, *J. Solid State Chem.* **177**, 3484 (2004).
- [41] F. M. Jaeger and W. A. Veenstra, *Recl. Trav. Chim. Pays-Bas* **53**, 677 (2010).